Proceedings of the Institute of Acoustics & Belgium Acoustical Society
Noise in the Built Environment, Ghent, 29-30 April 2010

COMPARATIVE STUDY OF THE EFFICIENCY OF ISOLATION MEASURES FOR VIBRATION AND NOISE FROM UNDERGROUND RAILWAY TRAFFIC

P. Fiala Budapest University of Technology and Economics, Dept. of Telecommunications
H. Verbraken K.U.Leuven, Department of Civil Engineering, Structural Mechanics
G. Lombaert K.U.Leuven, Department of Civil Engineering, Structural Mechanics
G. Degrande K.U.Leuven, Department of Civil Engineering, Structural Mechanics
F. Augusztinovicz Budapest University of Technology and Economics, Dept. of Telecommunications

1. INTRODUCTION

Underground traffic induced vibrations in dense urban environments can cause undesired effects in nearby buildings, as well as annoyance to the inhabitants. Vibrations are transmitted through the surrounding soil to nearby buildings, and induce structural vibrations that are dominant in the frequency range between 1 Hz and 80 Hz. Structural vibrations cause re-radiated noise in the building's enclosures, which is dominant in the frequency range between 30 Hz and 200 Hz. As the structural design process must involve the planning of vibration isolation systems that can mitigate structural vibrations and re-radiated noise, the accurate prediction of traffic induced vibrations and re-radiated sound is of high importance.

In the usual industrial design process, the design of the isolation structure and the required isolator quantity is based on simple design rules: The isolated structures, such as floating slab tracks, base isolated buildings or rooms with floating floors, are modeled by oversimplified (even SDOF) models, and the isolator quantity and quality is chosen based on prescribed isolation frequencies and insertion loss values computed from mass-spring systems.

This paper presents a parametric study on the performance of vibration and noise isolation of an office building exposed to ground-borne vibrations from a metro line. The parametric study is performed using a three-dimensional coupled numerical model that can model vibration and noise propagation starting from vibrations of a metro train running on an uneven rail and ending with the re-radiated sound in enclosures of a building structure. Two different countermeasures, such as a floating slab track at the source side and base isolation of the structure are modeled, and the performance of vibration and noise isolation computed by the numerical model is compared to the performance predicted by simple design formulas.

The structure of the paper is as follows: Section 2 briefly describes the key properties of the numerical model and introduces the modeled scenario. Section 3 presents the results of modeling the vibration and noise reduction on the source and receiver sides. Finally, Section 4 concludes the modeling results.

2. THE NUMERICAL MODEL AND THE MODELED SCENARIO

The geometry of the problem investigated is shown in figure 1. A straight underground railway tunnel is placed under a building resting on a layered half space. The origin of the Cartesian coordinate system is located at the center of the building's surface foundation, and the tunnel runs in the $y-$direction.

The total problem can practically be divided into three sub-problems.

2.1. The source problem

The first subproblem deals with the vibration generation into the soil by moving vehicles on an underground railway track.

Our source model consists of a distributed parameter track model coupled to a periodic finite element model of an invariant tunnel[1]. The surrounding soil is considered as a layered half space, and is modeled by a periodic boundary element method using the Green's functions of a layered half space [2, 3]. The Craig-Bampton substructuring technique is used to efficiently incorporate a track in the tunnel. The tunnel vibrations and radiated soil vibrations are computed in the frequency-wave number domain, and the

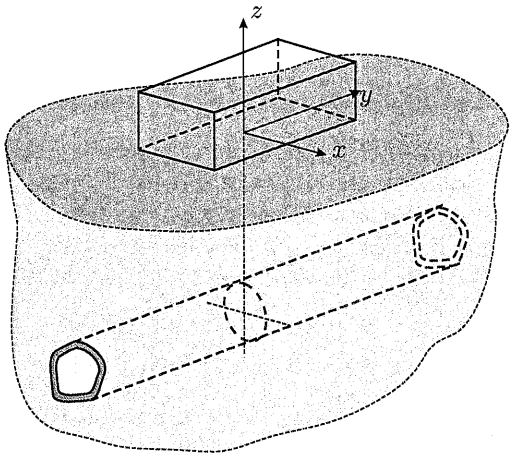

Figure 1: The problem geometry.

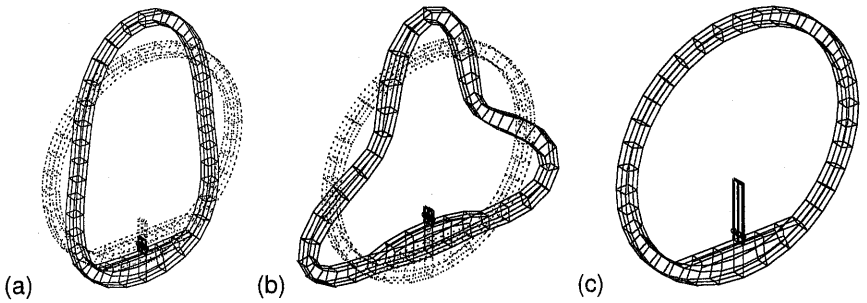

Figure 2: (a,b) The free tunnel modes and quasi-static transmission into the track and (c) a track mode on a rigid base.

Floquet transform technique is used to reduce the computation domain into a generic cell of the infinite, longitudinally invariant problem geometry [3].

An invariant tunnel embedded in a layered half space at a depth of 13.5 m is considered. The tunnel has an internal radius $r_i = 2.7$ m and a wall thickness $t = 0.3$ m. The tunnel has a concrete lining with a Young's modulus $E_t = 35000$ MPa, a Poisson's ratio $\nu_t = 0.25$, a density $\rho_t = 2500$ kg/m^3 and a hysteretic material damping ratio $\beta_t = 0.02$. A concrete slab is poured on the tunnel invert, which has a Young's modulus $E_t = 28500$ MPa, a Poisson's ratio $\nu_t = 0.2$, a density $\rho_t = 2500$ kg/m^3 and a hysteretic material damping ratio $\beta_t = 0.02$. The invariant tunnel is modeled as a periodic structure with a spatial period $L = 0.3$ m. The period of $L = 0.3$ m is chosen to keep the size of the finite element and boundary element mesh moderate, while not affecting the accuracy up to 150 Hz. The reference cell is discretized using 8-node volume elements with incompatibility bending modes. Figure 2 shows the tunnel modes at zero wavenumber, with their quasi-static transmission into the track and a track mode on a rigid base.

The layered half space consists of two layers with a thickness of 2 m and 18.5 m respectively, on top of a half space. The top layer has a shear wave velocity $C_s = 180$ m/s and a material damping ratio $\beta_s = 0.03$, while the second layer is stiffer and has a shear wave velocity $C_s = 220$ m/s and a material damping ratio $\beta_s = 0.025$. The underlying half space has a shear wave velocity $C_s = 320$ m/s and a material damping ratio $\beta_s = 0.0225$. A Poisson's ratio $\nu_s = 0.33$ and a density $\rho_s = 2000$ kg/m^3 is assumed in all layers.

A conventional non-ballasted concrete slab track is considered in the tunnel. UIC 60 rails are used that have a cross-sectional area $A_r = 7.672 \times 10^{-3}$ m^2, a moment of inertia $I_r = 3.039 \times 10^{-5}$ m^4, a mass per unit length $\rho_r A_r = 60.22$ kg/m and a bending stiffness $E_r I_r = 6.382 \times 10^6$ Nm^2. Soft rail pads with a stiffness $k_{rp} = 50$ MN/m discretely support the rails at an interval $d = 0.6$ m on the sleepers. The concrete

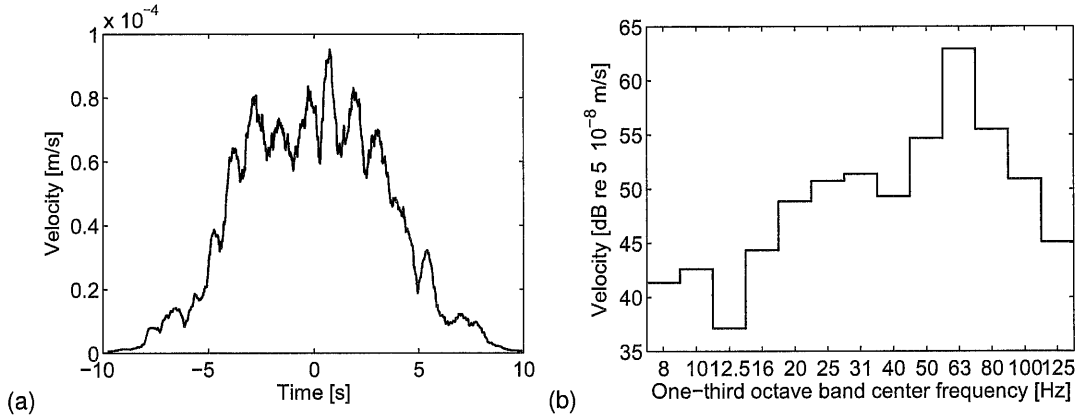

Figure 3: (a) Running RMS and (b) one-third octave band spectrum of the vertical component of the free field velocity at the center of the surface foundation due to the passage of the train in the tunnel at a speed of 50 km/h. Black line: unisolated case, gray line: isolation with a floating slab track.

sleeper has a mass $M_s = 200$ kg. The track is modeled as an infinite beam on continuous support. The model consists of an infinite Euler beam, representing the (two) rails and the mass elements representing the sleepers. The mass of the sleepers is distributed in the longitudinal direction with a mass per unit length $m_s = M_s/d = 333$ kg/m. The rail pads are modeled as a continuous support with vertical stiffness $\bar{k}_{rp} = 2k_{rp}/d = 166.6\,\text{MN/m}^2$ between the beam and the sleepers, while the rigid connection between the sleepers and the concrete slab is modeled with very stiff springs below the mass elements.

A metro train traveling with a speed of 50 km/h on an uneven rail is modeled. The train consists of seven cars each of length 16 m. The bogie and axle distance on all cars are 10.34 m and 1.91 m, respectively. The mass of the coach with passengers is 43000 kg, while the mass of the bogie and axle are 3600 kg and 1700 kg, respectively.

The dynamic interaction between the wheel and the rail is responsible for generating vibrations from moving trains. In this paper, two excitation mechanisms are considered: the quasi-static excitation and the unevenness excitation.

The rail unevenness $u_{w/r}(y)$ is expressed as a stochastic process characterized by a single-sided power spectral density (PSD) $\tilde{G}'_{w/r}(n_y)$ written as a function of the cyclic wavenumber $n_y = f/v = 1/\lambda_y$:

$$\tilde{G}'_{w/r}(n_y) = \frac{A' n_{y2}^2 (n_y^2 + n_{y1}^2)}{n_y^4 (n_y^2 + n_{y2}^2)} \tag{1}$$

where $n_{y1} = 0.0233$ cycle/m and $n_{y2} = 0.1312$ cycle/m. In this paper, the roughness parameter is selected as $A' = 16.72 \times 10^{-7}$ m cycle. An artificial roughness is generated from this PSD curve and the frequency content of the roughness is determined for a particular speed [4].

Figure 3 shows the running RMS time history and one-third octave band spectrum of the vertical component of the free field velocity at the origin of the coordinate system. The running RMS time history is computed by a time window length of 0.5 s. The passage of the seven cars is clearly visible in the curves. The one-third octave band RMS spectrum of the vertical velocity is computed according to the German standard DIN 45672-2 [5] on a reference period T_2, during which the response is considered to be stationary. The dominant part of the frequency content is between 10 and 80 Hz, which gives rise to low-frequency vibrations and re-radiated noise in the buildings. The higher frequency components up to 150 Hz are also present but are considerably attenuated due to the material damping in the soil. The peak in the frequency content around 55 Hz corresponds to the wheel-track resonance frequency. The passage of the individual axles of the train is not apparent in the time history, as the contribution of the quasi-static forces is negligible in the free field and the dynamic forces due to the rail unevenness dominate.

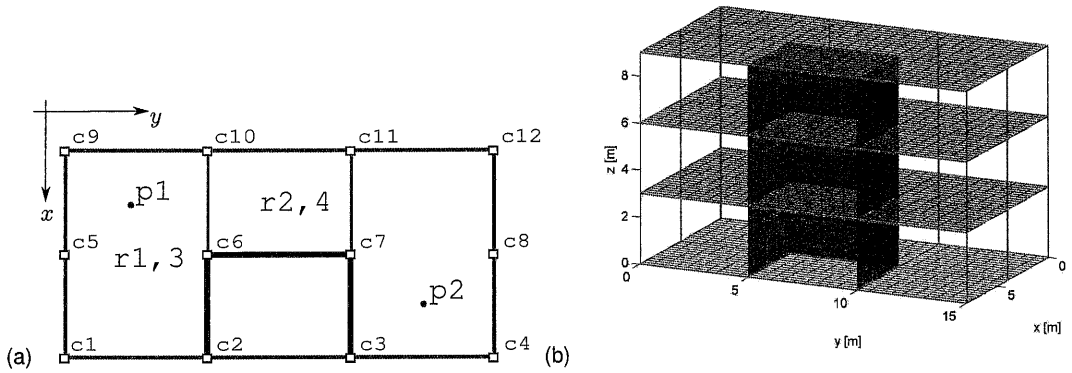

Figure 4: (a) Ground plan of the structure model with indicating the column numbering cn, two observation points p1 and p2 and the room setup rn. The solid black line indicates the core walls, the thick and thin gray lines denote the external and internal masonry walls, respectively. (b) Finite element model of the structure

2.2. The structural response

The second subproblem is the dynamic soil-structure interaction problem, where the incident wave field is applied as an excitation to a coupled soil-structure model and the structural vibrations are determined. In the present case, the structural vibrations due to the incident wave field are computed by means of a three-dimensional coupled finite element-boundary element model, based on the subdomain formulation proposed by Aubry and Clouteau [6]. The dynamic stiffness of the soil and the dynamic loads resulting from the incident displacement wave field are computed using a three-dimensional boundary element method [7] in the frequency domain, using the Green's functions of a layered half-space [8]. The Craig-Bampton substructuring [9] is used to differentiate between the foundation modes and their quasi-static transmission into the building, and the modes of the superstructure on rigid base [10].

The modeled structure is a three-story portal frame office building located directly above the tunnel. The dimensions of the building are 15 m $\times$ 8 m $\times$ 9 m in the x, y and z directions, respectively. The structure is modeled by means of a three-dimensional structural finite element method. The ground plan of the modeled structure and its finite element mesh is plotted in Fig. 4. The finite element mesh does not show the external masonry walls, although they are incorporated in the model.

The structure rests on a 30 cm thick reinforced concrete surface raft foundation. The basic structure of the building contains the columns and beams of the portal frame structure, as well as the slabs covering the three levels. All columns and beams have a rectangular cross section with dimensions 0.3 m $\times$ 0.3 m, the slabs have a thickness of 0.3 m.

The columns are placed regularly, so they split the ground plan of each level into 2×3 sections of identical size: The dimensions of one section are 4 m $\times$ 5 m. One of the central sections is surrounded from three sides by the structure core walls. The core walls are modeled as 0.2 m thick reinforced concrete slabs.

All the external and some internal masonry walls are also taken into account in the finite element model. The thickness of the external and internal walls are 12 cm and 6 cm, respectively. The total dead mass of a story is 136 t, the mass of the superstructure is 407 t.

Figure 5. displays the RMS time history and one-third octave band levels of the vertical structural velocity at two points P1 and P2 of the first slab. The two observation points are at coordinates ($x = 2$ m, $y = 2.5$ m) and ($x = 6$ m, $y = 12.5$ m), and are also displayed in Fig. 4. The RMS curves are computed from the time histories with a time window of length 0.5 s. Note that although both observation points are located at the central point of a superstructure segment, the RMS vibration histories show a difference of 6 dB. Again, as for the case of the incident wave field, the dominant frequency bands are around 50-60 Hz.

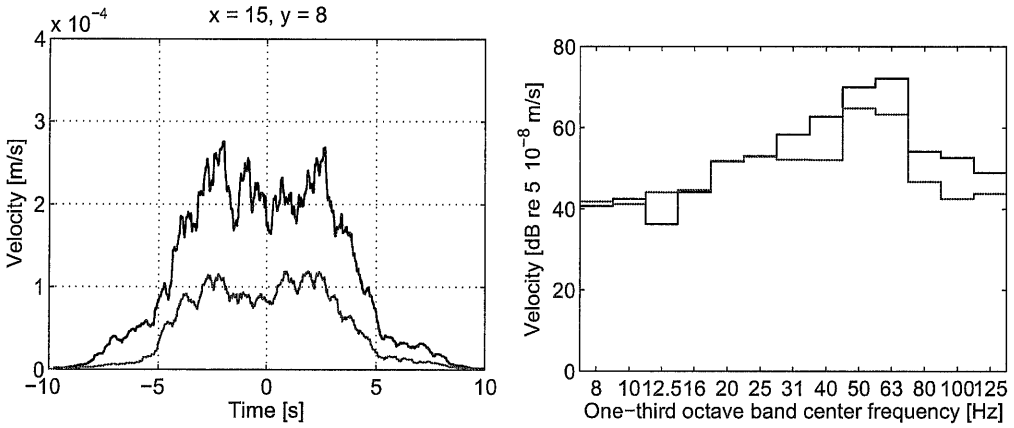

Figure 5: RMS time history and one-third octave band spectra of the vertical velocity in point P1 (black) and P2 (gray) of the first slab of the superstructure.

n	1	2	3	4	5	6	7	8	9	10	11	12	13	14
$f_{n,\text{large}}$	21.4	34.3	40.4	42.8	54.9	57.1	61.0	64.3	66.6	68.6	70.0	71.4	71.8	72.8
$f_{n,\text{small}}$	34.3	42.8	54.9	57.1	66.6	68.6	71.4	79.2	80.8	85.7	89.2	92.3	99.0	102.9

Table 1: Eigenfrequencies of the first few dynamic modes of the small and large rooms expressed in Hz

2.3. The acoustic model

In the third subproblem, the radiation problem is solved, where the sound pressure radiated into the closed rooms of the structure by vibrating walls is determined. For typical room dimensions, the upper frequency limit is not much higher than the eigenfrequency of the first few acoustic modes. Therefore, deterministic models can handle the noise radiation problem.

The re-radiated noise in the building's enclosures is computed by means of an acoustic spectral element method applied to rectangular rooms [11]. The coupling between structural vibrations and the acoustic field is determined by the acoustic impedance of the walls; these values are approximated using acoustic absorption coefficients of different acoustic materials.

The computation of the acoustic response radiated into closed rooms by vibrating walls and floors involves the solution of the Helmholtz equation in closed rectangular spaces. As the impedance of the radiating walls is much larger than that of the internal acoustic space, a weak coupling between structural and acoustic vibrations is assumed: The acoustic pressure inside the room has no effect on the vibration of the walls and the computed structural vibration velocity is applied as a boundary condition in an acoustic boundary value problem.

The internal acoustic spaces are characterized by the material properties of the sound: mass density of the air $\rho_a = 1.225$ kg/m^3 and speed of sound $C_a = 343$ m/s. The wall surfaces are characterized by acoustic impedance values. At relative low frequencies, the acoustic impedance can be computed from the walls' acoustic absorption coefficient α, which gives the ratio of the absorbed and the incident acoustic energy when a normal incident acoustic plane wave is reflected from the surface.

In the present model, four rooms are modeled, rooms (r1 and r2) being on the first floor, and the same room setup (r3 and r4) is repeated on the second floor. The room setup has already been shown in Fig. 4. The two large rooms are of dimensions $8 \times 5 \times 3$ m, while the small room is $4 \times 5 \times 3$ m. The room dimensions and material properties of the air determine the resonance frequencies of the cavities. For the case of the larger rooms, the first resonance frequencies are listed in Tab. 1. The absorption coefficient is assumed to have a constant value $\alpha = 10\%$ for all rooms of the structure.

Different measures are applied to characterize the sound pressure in different rooms of the structure.

- As a local measure, the one-third octave band sound pressure level $P(\mathbf{x}, \omega_\mathbf{k})$ is evaluated in different positions inside the cavities.

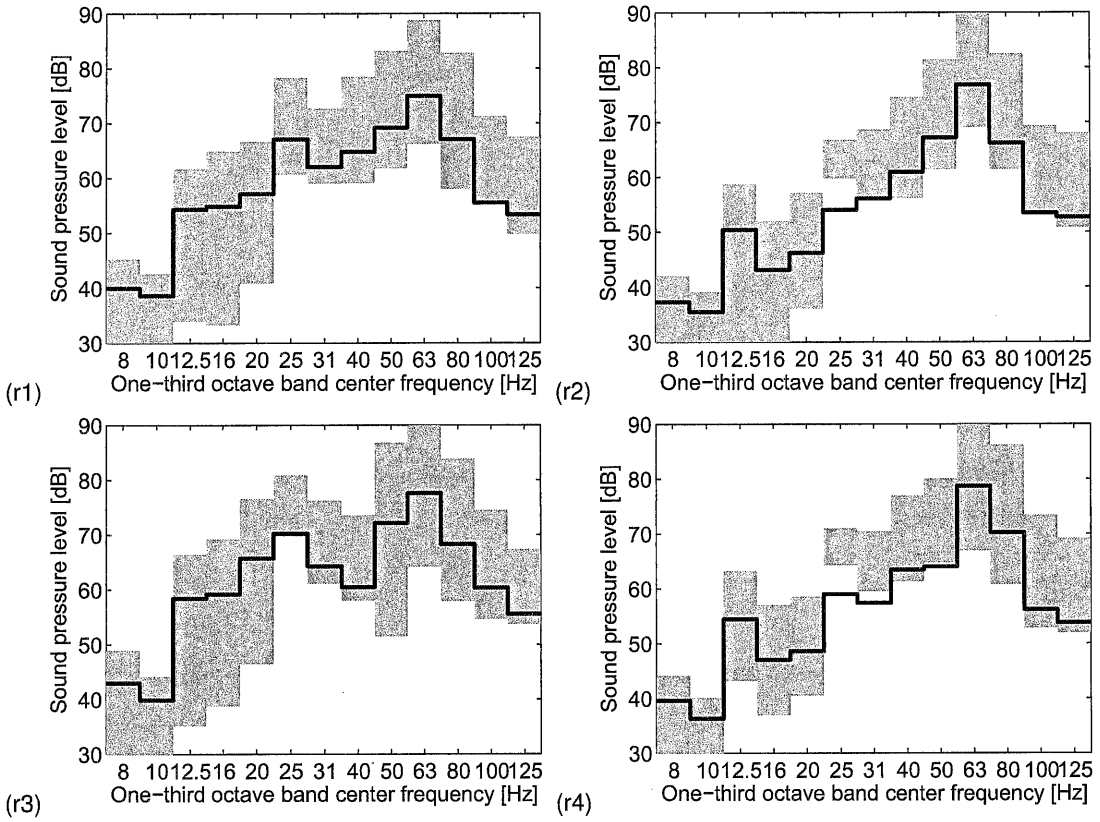

Figure 6: Sound pressure level and sound energy in four rooms of the structure. The gray patch displays the range of the sound pressure $P(\mathbf{x}, \omega_k)$ over the whole room volume, the thick black line displays the sound energy level $E_a(\omega_k)$.

- As a global measure, the total one-third octave band acoustic sound energy $E_a(\omega_k)$ inside the rooms is evaluated for each frequency band, and is compared for the isolated and unisolated cases.

The different measures are displayed in Fig. 6 for the case of the four rooms of the structure. In the figures, the gray patch shows the range of the local sound pressure $P(\mathbf{x}, \omega_k)$ over the whole room volumes, the thick black line displays the sound energy level $E_a(\omega_k)$. For the case of the larger rooms, the dominant one-third octave bands are clearly the 25 Hz and the 63 Hz bands. This is partly due to the excitation velocity that is dominant in these frequency bands (as shown in Fig. 5), and also due to the coincidence with the first horizontal and vertical acoustic eigenfrequencies amplifying the peaks in the mentioned frequency range. For similar reasons, the dominant bands are the 50 Hz and 63 Hz bands for the smaller room dimensions.

Due to the presence of several acoustic resonance peaks and dips in the investigated frequency range, the local sound pressure levels are distributed in a rather wide, ($\approx 15-20$ dB) level range. This implies that evaluating the local sound pressure in a few positions can be misleading when evaluating the governing sound pressure level in rooms. The difference between the sound energy levels in the different floors is negligible.

3. VIBRATION AND NOISE ISOLATION

3.1. Vibration isolation by means of a floating slab track

The isolation of the source is considered to mitigate the vibrations induced by moving trains. This has an advantage with respect to the isolation at the receiver side that it affects several structures in the surround-

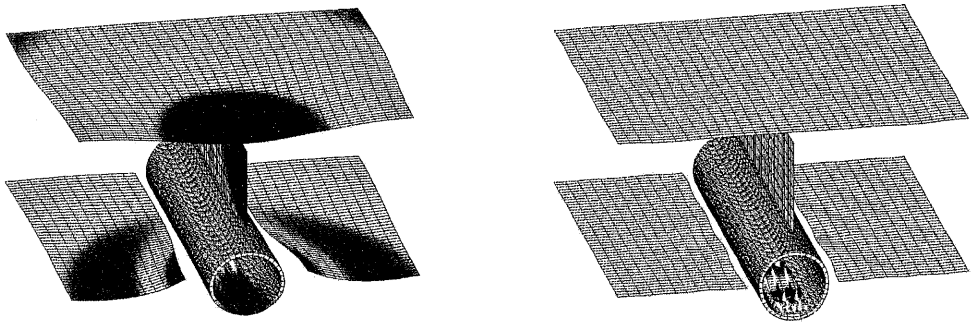

(a) (b)

Figure 7: Real part of the vertical displacement of the tunnel and the soil due to a harmonic excitation on the floating slab track at (a) 10 Hz and (b) 60 Hz.

ing.

In this paper, the vibration isolation efficiency of a floating slab track with an isolation frequency of 10 Hz is investigated. The isolation frequency of the floating slab track is defined as the resonance frequency of a single-degree-of-freedom system with a mass equal to the track's mass per unit length and stiffness equal to the vertical stiffness of the slab bearings. Discontinuous concrete slabs of dimensions 31 m $\times$ 2.5 m $\times$ 0.45 m are supported by two rows of 17 springs with a spring stiffness of 10 MN/m each. The slab is modeled as a continuous beam coupled to the tunnel via a uniform support, that has a low stiffness corresponding to the isolation frequency of 10 Hz.

Figure 7 shows the displacements of the tunnel and the soil for a harmonic excitation at 10 Hz and 60 Hz after the installation of a 10 Hz floating slab in the tunnel. The floating slab track allows the energy to propagate along the slab instead of being transmitted to the tunnel and the soil. At the excitation frequency of 10 Hz, resonance is observed, amplifying the displacements in the track, the tunnel and the soil. At the excitation frequency of 60 Hz, there is a significant reduction in the displacements of the tunnel and the soil, while the response of the track has increased and may result in larger vibrations and noise in the tunnel and the train.

Figure 8 shows the one-third octave band spectrum of the insertion loss of the the floating slab, expressed using the vibration velocity on the surface foundation. The gray curve displays the insertion loss derived from a simple single degree of freedom system consisting of the mass of the track-slab system and the stiffness of the springs supporting the floating slab. This curve is negative in the first two one-third octave bands around the 10 Hz isolation frequency, and increases with a slope of 40 dB per decade above the resonance.

For the case of a distributed system, the vibration velocity insertion loss can not be expressed by a single number; its value depends on the location over the surface foundation. The insertion loss is the largest at those locations that are directly above the tunnel, and its value decreases with increasing distance from the tunnel's vertical symmetry plane. The range of the insertion loss over the whole foundation is plotted with a light gray patch in the figure, its mean value is marked by the black curve. It is noted that even the maximum of the computed IL's range deviates from the IL of the SDOF system; the difference is about 15 dB around 100 Hz. This difference is due to the finite extent of the vibration source in both horizontal directions.

3.2. Base isolation

In order to reduce ground-borne vibration and noise in the building, base isolation is applied. As a usual choice, the isolation cut is planned between the surface foundation and the columns of the first floor. By this choice, the whole superstructure is isolated from the vibrations of the ground and the foundation. However, the maximal superstructure load is taken up by the isolators, what increases the required isolator quantity and construction costs.

In the usual design process, the required isolator quantity and setup is determined using simple design

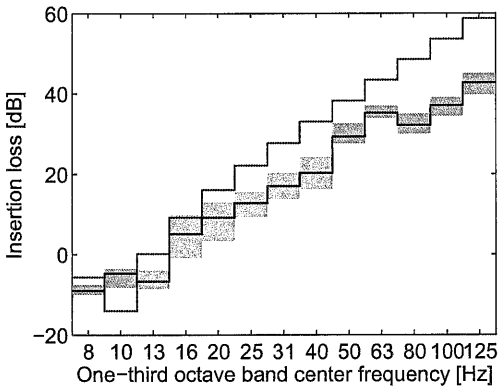

Figure 8: Insertion loss of the 10 Hz floating slab track derived from the vertical vibrations at the surface foundation. The gray patch shows the range of the insertion loss over the whole foundation surface, the black curve indicates its mean value. The gray line shows the theoretical insertion loss curve expected from a SDOF system.

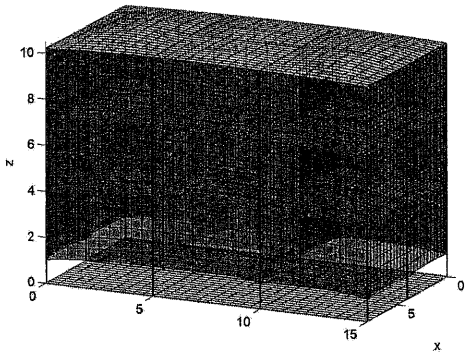

Figure 9: Dynamic mode of the superstructure resting on a clamped foundation at $f = 9.4$ Hz

rules, based on information on the static load at the vibration cut, the available support surface at the vibration cut, and the required performance expressed as a desired isolation frequency.

In the present case, the vertical and horizontal static dead loads G_v and G_h at the bottom of the twelve ground floor columns have been determined from the finite element model, and are listed in Tab. 2. The live load resulting from all movable weights was not taken into account in the present model. The support surface is $0.3\ \mathrm{m} \times 0.3\ \mathrm{m}$ for all the twelve columns. The desired performance is defined as an isolation frequency $f_{\mathrm{iso}} \approx 10$ Hz.

The isolators are realized in the form of simple elastomer bearings. All the elastomer parameters are selected from catalogue data. The isolators are realized as elastomer cubes with unloaded dimensions $10\ \mathrm{cm} \times 10\ \mathrm{cm} \times 5\ \mathrm{cm}$. The elastomer cubes are designed for 10 Hz isolation frequency with 60 kN static load and 11 mm static deflection. (The vertical static stiffness of an elastomer element is $5.45\ \mathrm{kN/mm}$, the vertical dynamic stiffness under design load conditions is $23.6\ \mathrm{kN/mm}$).

The necessary bearing quantity per column is reached by using blocks of elastomer elements placed in a regular $m \times n$ structure, with a spacing of 15 mm, to enable horizontal deformation (Poisson-effect). The number of elastomer elements placed under the columns of the structure is also listed in Tab. 2.

In the finite element model, the bearings are modeled as simple spring elements with the appropriate dynamic stiffness connecting the translational DOF of the columns to that of the supporting foundation slab. The horizontal and vertical dynamic stiffnesses are considered to be the same.

Figure 9 displays the vertical translational resonance mode mode of the superstructure resting on a

Table 2: Vertical G_v and horizontal G_h static load and number of elastomer elements n_b at the columns of the base isolated superstructure.

#column	1, 4	2, 3	5, 8	6, 7	9, 12	10, 11
G_v [kN]	185	415	220	687	222	308
G_h [kN]	26	108	3	142	33	24
n_b	2×2	2×3	2×2	3×4	2×2	2×3

clamped foundation at 9.4 Hz.

The actual performance of base isolation for the mitigation of traffic induced ground-borne vibrations is evaluated using different local and integrated measures:

- The time history of the vertical RMS velocity $v_z(\mathbf{x}_i, t)$ at specific locations $\mathbf{x}_i$ of the superstructure's slabs is compared for the case of the isolated and unisolated cases.
- The one-third octave band RMS-spectra $V_z(\mathbf{x}_i, \omega_k)$ of the vertical slab vibration velocity is evaluated in different locations $\mathbf{x}_i$, and is compared between the cases with and without isolation. Comparison is quantified by evaluating the local vertical velocity insertion loss IL^{V_z} at specific locations $\mathbf{x}_i$ and each one-third octave band ω_k. The velocity insertion loss is defined as

$$\mathrm{IL}^{V_z}(\mathbf{x}_i, \omega_k) = 20 \log_{10} \frac{V_z^{\text{uniso}}(\mathbf{x}_i, \omega_k)}{V_z^{\text{iso}}(\mathbf{x}_i, \omega_k)} \tag{2}$$

- As an integrated measure, the total vibration energy $E(\omega_k)$ of the individual superstructure slabs is evaluated at each one-third octave band ω_k, and is compared between the cases with and without isolation. The comparison is quantified as an energy insertion loss IL^E defined as

$$\mathrm{IL}^E(\omega_k) = 10 \log_{10} \frac{E^{\text{uniso}}(\omega_k)}{E^{\text{iso}}(\omega_k)} \tag{3}$$

Fig. 10 displays the insertion loss of base isolation using local and integrated measures. The figure shows the energy insertion loss IL^E for the case of the three superstructure slabs with a solid black line. The gray patch displays the range of the velocity insertion loss $\mathrm{IL}^{V_z}(\mathbf{x}_i)$, when $\mathbf{x}_i$ takes an arbitrary value over the slab surfaces. It is clearly visible that the the local indicator varies intensively, and single curves selected at a single location can be misleading when evaluating the performance of base isolation.

The figures also compare the actual insertion losses with that predicted by an SDOF system consisting of the mass of the superstructure and the total stiffness of the isolation bearings. The results show that the SDOF system gives a good estimate of the performance near the resonance frequency, but in the higher frequency range, the isolation effect is highly overestimated: The energy insertion loss predicted from the numerical model hardly exceeds the limit of 20 dB, even at frequencies two decades higher than the resonance frequency.

The large difference may be explained with the dynamics of the superstructure. The portal frame three-story building can be modeled as a rigid mass near the resonance frequency, but not in the high frequency range, where the local modes of the slabs, core and masonry walls dominate in the response.

3.3. Comparison of the countermeasures

Finally, the performance of the two countermeasures is compared in Figure 11. The comparison is based on the acoustic response in room 2, and is quantified in the form of insertion losses:

- The solid black line shows the acoustic energy insertion loss $\mathrm{IL}^{E_a}(\omega_k)$ that is computed in a similar manner as the structural energy insertion loss in equation (3)
- The gray patch displays the range of the sound pressure insertion loss $\mathrm{IL}^P(\mathbf{x}, \omega_k)$ that is computed in a similar manner as the structural energy insertion loss in equation (2)

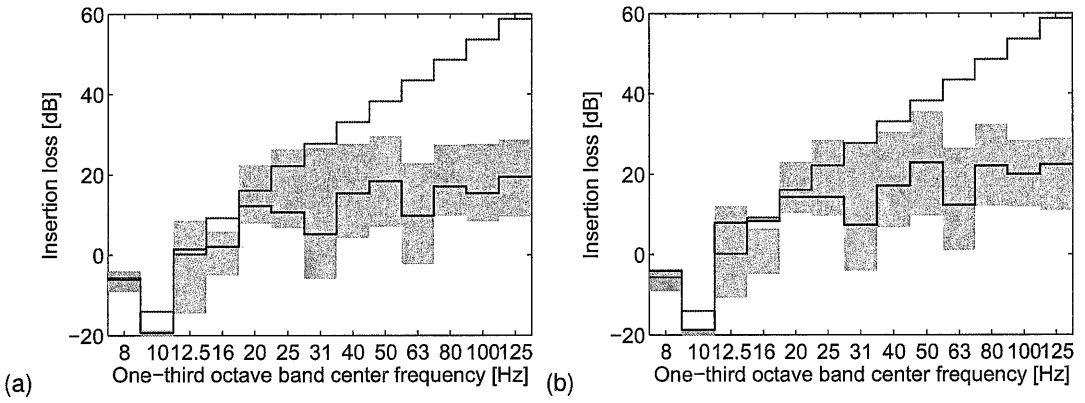

Figure 10: Performance of base isolation in one-third octave bands for (a) the first and (b) the second slab of the superstructure. The solid black line shows the energy insertion loss IL^{E}, the gray patch displays the range of the vertical velocity insertion loss IL^{V_z} over the whole slab surface, and the gray solid curve shows the insertion loss predicted from a SDOF system.

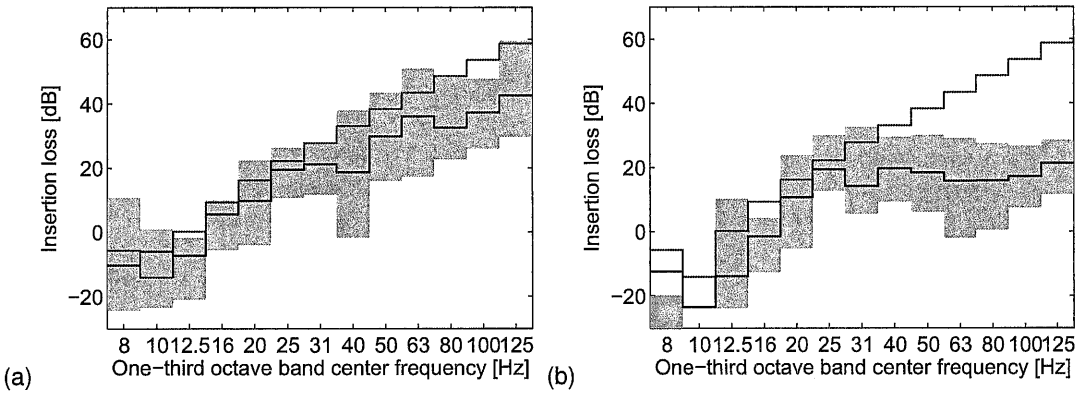

Figure 11: Insertion loss of (a) the floating slab track and (b) the base isolation computed from the sound pressure field in room 2. The solid black line shows the acoustic energy insertion loss IL^{E_a}, the gray patch displays the range of the sound pressure insertion loss IL^{P} over the whole room volume, and the gray solid curve shows the insertion loss predicted from a SDOF system.

- The gray solid curve shows the insertion loss predicted from a SDOF system.

The results show that the acoustic insertion loss of the floating slab is close to that of the SDOF system, but the deviation between the SDOF curve and the energy insertion loss curve reaches 20 dB above 100 Hz. For the case of the base isolation, the acoustic insertion loss IL^{E_a} is very close to the structural energy insertion loss presented in Fig. 10.

4. CONCLUSIONS

A numerical model has been used to compute structural vibrations and re-radiated noise in buildings generated by underground railway traffic. The model is a deterministic three-dimensional approach, accounting for vibration generation by a moving train on periodic media, dynamic soil-structure interaction and sound radiation into closed rooms.

The methodology has been used to demonstrate the efficiency of two vibration and noise reduction methods: a floating slab track and base isolation. The countermeasures are assessed by calculating the insertion loss on the re-radiated noise.

The floating slab track has been found to be a very effective vibration and noise reduction mechanism. This method provides the largest amount of vibration reduction in the investigated building, and it yields a vibration reduction at the source, which is advantageous to all the structures around the metro line.

It has been found that base isolation of the structure can result in significant (> 20 dB) vibration isolation over all the building, but, for the case of complex structures, the isolation effect is considerably less than predicted by SDOF models. This conclusion is significant, as mass-spring systems form the basis of the design of base isolation systems in many practical cases.

For both kinds of vibration and noise isolation strategies, local and global measures have been used to assess the efficiency of the reduction. For the case of the base isolation, it has been shown that local measures may be misleading in the characterization of noise isolation performance.

The use of advanced prediction models prospers a better understanding in the generation and propagation mechanism of ground-borne noise and vibration and allows for studying the effect of structural changes on the source as well as the receiver side. Simple numerical models can be used to make rational decisions about the design of vibration isolation systems, however, it is worthwhile to verify the design using state-of-the-art three-dimensional models.

ACKNOWLEDGMENTS

The authors are grateful to Ir. M. Vanstraelen from CDM for providing useful technical information on base isolation systems.

References

[1] S. Gupta, G. Degrande, H. Chebli, D. Clouteau, M.F.M. Hussein, and H. Hunt. A coupled periodic fe-be model for ground-borne vibrations from underground railways. In Mota Soares C.A., editor, *Proceedings of the 3th European Conference on Computational Mechanics*, Lisbon, Portugal, June 2006.

[2] D. Clouteau, M. Arnst, T.M. Al-Hussaini, and G. Degrande. Free field vibrations due to dynamic loading on a tunnel embedded in a stratified medium. *Journal of Sound and Vibration*, 283(1–2):173–199, 2005.

[3] G. Degrande, D. Clouteau, R. Othman, M. Arnst, H. Chebli, R. Klein, P. Chatterjee, and B. Janssens. A numerical model for ground-borne vibrations from underground railway traffic based on a periodic finite element - boundary element formulation. *Journal of Sound and Vibration*, 293(3-5):645–666, 2006. Proceedings of the 8th International Workshop on Railway Noise, Buxton, U.K., 8-11 September 2004.

[4] G. Lombaert, G. Degrande, J. Kogut, and S. François. The experimental validation of a numerical model for the prediction of railway induced vibrations. *Journal of Sound and Vibration*, 297(3–5):512–535, 2006.

[5] Deutsches Institut für Normung. *DIN 45672 Teil 2: Schwingungsmessungen in der Umgebung von Schienenverkehrswegen: Auswerteverfahren*, 1995.

[6] D. Aubry and D. Clouteau. A subdomain approach to dynamic soil-structure interaction. In V. Davidovici and R.W. Clough, editors, *Recent advances in Earthquake Engineering and Structural Dynamics*, pages 251–272. Ouest Editions/AFPS, Nantes, 1992.

[7] D. Clouteau. *MISS Revision 6.2, Manuel Scientifique.* Laboratoire de Mécanique des Sols, Structures et Matériaux, Ecole Centrale de Paris, 1999.

[8] J.P. Wolf. *Dynamic soil-structure interaction.* Prentice-Hall, Englewood Cliffs, New Jersey, 1985.

[9] R.J. Craig and M. Bampton. Coupling of substructures for dynamic analyses. *AIAA Journal*, 6(7):1313–1319, 1968.

[10] P. Fiala, G. Degrande, and F. Augusztinovicz. Numerical modelling of ground-borne noise and vibration in buildings due to surface rail traffic. *Journal of Sound and Vibration*, 301:718–738, 2007.

[11] P. Fiala. *Development of a Numerical Model for the Prediction of Ground-borne Noise and Vibration in Buildings*. PhD thesis, Budapest University of Technology and Economics, Budapest, 2009.